Analyzing Power Oscillating Signals With the O-Splines of the Discrete Taylor–Fourier Transform

José Antonio de la O Serna ⓘ, *Senior Member, IEEE*

Abstract—Power oscillating signals are analyzed with the Discrete Taylor–Fourier Transform (DTFT). This is implemented by modulating the impulse responses of its low-pass differentiators, defined by a family of O-splines. This implementation reduces its computational complexity since in practice only a small subset of filters is applied. The estimated parameters provide richer dynamic information than the traditional methods, in particular, a space representation for each dynamic component, and detection of frequency modulated events. Their estimation performance is assessed through the new proposed Total Phasor Error. To illustrate its application, and its progressive accuracy, this technique is applied to observe the synchrophasor estimates of voltages and to separate the electromechanical modes of an oscillation in a real power system. In conclusion, this multiresolution technique provides a series of increasingly precise solutions for time-frequency separation of oscillations with fluctuating frequency.

Index Terms—Discrete Taylor–Fourier transform, dynamic phasor, electromechanical modes, envelope detection, filter banks, multi-resolution analysis, oscillory harmonics, O-splines, phase space, power oscillations, synchrophasor estimation, time-frequency separation, total phasor error.

I. INTRODUCTION

MEASUREMENT of power system oscillation signals is considered in the literature as two independent problems. On the one side, there are many studies for implementing better algorithms to measure synchrophasors of voltages and current signals under oscillations for the phasor measurement units (PMU) installed in smart grids of wide area networks. On the other side, abundant literature exists dedicated to improving the analysis of electromechanical modes in power swings. In this paper, we propose the O-splines of the Discrete Taylor-Fourier Transform (DTFT) to solve both important power system problems.

These problems have in common signal components with dense spectral energy about certain frequencies: around harmonic frequencies in the first case, and about the mode frequencies in the second one. The basic problem of the Discrete Fourier Transform (DFT), in dealing with dense spectral components, is that it distorts amplitude and phase [1]. DFT works accurately only when signals have constant amplitude, phase,

and frequency. DTFT solves this impairment by substituting each DFT constant Fourier coefficient by a Taylor polynomial of Kth degree during the time observation window.

Larger Taylor-Fourier subspaces are spanned by including Taylor terms of higher order at each harmonic component of the Fourier basis [2]. Since Taylor polynomials of higher degree include those of lower degree, each Taylor term included in the signal model makes the subspace gradually grow from the previous one. Taylor polynomial extensions span a ladder of spaces that better and better approximate ideal bandpass signals. They start with the coarser one, defined by the constant complex coefficients of the DFT, in which the periodic signals live. By adding more and more Taylor terms to the signal model, vaster subspaces are spanned, containing the previous ones. Therefore, the DTFT subspaces deliver better and better approximations to oscillatory signals, and estimated dynamic parameters with smaller and smaller errors. As a consequence, the estimates obtained with higher degrees are always more accurate than those obtained with lower degrees in oscillatory signals.

In this paper, the estimated parameters by the first and third degree Taylor polynomials are compared. In addition, it is demonstrated that the impulse responses of the DTFT filters are simply modulations at the harmonic frequencies of the impulse responses of the lowpass filters. Therefore, our focus is centered on the lowpass differentiators, which are defined by a new set of splines, i.e. piecewise-functions defined by polynomials. In our case, each cycle of the impulse responses is defined by a different Taylor polynomial. For this reason, they will be referred to as cyclic- or O-splines.

On the spectral side, the Taylor extension widens and flattens the mainlobe of the DTFT filters. As a result of this relaxation, the DTFT is more suitable to measure oscillatory harmonics. In the decomposition side, the DTFT is endowed with a filter bank with maximally flat ideal differentiator gains at their passband, and zero-flat gain at their stopbands at the rest of harmonic frequencies. Thus, at each harmonic frequency, they act as ideal differentiators, with perfect harmonic rejection at the rest of them.

Concerning the synchrophasor estimation application, it is worth to mention that the synchrophasor standard [3] was written under the strong influence of the traditional single-cycle DFT estimator [4]. Now the emphasis of the standard is put on the effect of the noise in the estimates [5]. But the paradigmatic role of the Fourier filter is persistently defended despite its known limitations under oscillatory conditions (the infiltration of the image frequency, and the scalloping loss due to its uneven

passband gain) [6], [7]. That is why, after recognizing the good steady-state regulation of the IEEE Synchrophasor Standard, the Western Electricity Coordinating Council (WECC) [8] has proposed better dynamic performance requirements for PMU filters, to guarantee better responses under dynamic conditions, such as power swings or changing harmonics. An adaptive complex bandpass filter derived from the exponentially modulated filter bank theory was proposed with 4- and 7-cycle impulses responses, and frequency variations ranging from 40 to 80 Hz. Here the series of impulses responses of the DTFT passband differentiators are proposed to observe the dynamics of oscillating signals. The provided solutions can be gradually chosen to improve the accuracy of the estimates, starting from the coarser DFT itself, and ending with better and better optimal representations for protections (P) and measurement (M) class applications.

On the other hand, the identification of electromechanical modes in power oscillations has been studied by many researchers through the following main approaches [9]: linear ring down analysis [10], [11], mode meter analysis [12], and nonlinear analysis [13], [14]. Those methods (Prony, Yule Walker, and Hilbert Wang) consider modes as wide band components located anywhere in the spectral side, while DTFT [15] partitions frequency in a set of disjoint passband intervals from which the complex envelope of each oscillation mode is observed through its Taylor decomposition. It provides time-frequency separation of modes with fluctuating frequency, and a phase space parametrization for the dynamics of each mode. Of course, the central frequency of the DTFT filters must be tuned [16] to the mean central frequency of each mode. The example analyzed in Section IV illustrates the new parametrization provided by the DTFT analysis.

In the following, signal models of Taylor-Fourier subspaces are presented in Section II, with the impulse responses of the filters, and their frequency responses. This is done for the first three passband differentiators. In Section III are shown the pointwise DTFT dynamic phasors, estimated with first and third degree Taylor polynomials, and obtained from the voltage signals during an oscillation hit by a fault. Instantaneous amplitude, phase and frequency estimates are illustrated to show the accuracy improvement. Finally, in Section IV, DTFT is used to separate the electromechanical modes of the power oscillation. The analysis illustrates the amplitude and phase estimates of the first two modes, together with their first derivative. It concludes for both applications that DTFT enriches the parametric representation of those complex dynamic events.

II. DIGITAL TAYLOR-FOURIER SUBSPACE

The expansion from the static to the dynamic phasor and its derivatives was originally presented in [17]. This led to the extension from the Fourier subspace to the Taylor-Fourier subspaces as presented in [18]. This extension can be briefly introduced, by starting from the zeroth-order traditional Fourier signal model

$$x_0 = \Phi_0 \xi_0, \qquad (1)$$

where Φ_0 is the $N \times N$ Fourier matrix W_N, and ξ_0 contains the Fourier coefficients of x_0. The elements of W_N are $w_{nk} = e^{j\frac{2\pi}{N}kn}$, for $n, k = 0, 1, \ldots, N-1$, where N is the number of samples per fundamental cycle.

We extend the former subspace by including the first Taylor term. The signal model for this first extension is then:

$$x_1 = \Phi_1 \xi_1$$

$$= \left(I \begin{pmatrix} W_N \\ W_N \end{pmatrix} \quad T \begin{pmatrix} W_N \\ W_N \end{pmatrix} \right) \begin{pmatrix} \xi_N \\ \dot{\xi}_N \end{pmatrix} \qquad (2)$$

where the diagonal matrices I and T contain the samples of the zeroth and first Taylor terms, respectively, taken in two-cycle-long centered intervals. And the subvector $\dot{\xi}_N$ contains the derivatives of the first Taylor-Fourier coefficients in ξ_N.

The following extensions are obtained by including more and more Taylor terms. The signal model for the K-th extension is as follows:

$$x_K = \Phi_K \xi_K$$

$$= \left(I \begin{pmatrix} W_N \\ W_N \\ \vdots \\ W_N \end{pmatrix} \quad T \begin{pmatrix} W_N \\ W_N \\ \vdots \\ W_N \end{pmatrix} \quad \cdots \quad \frac{1}{K!}T^K \begin{pmatrix} W_N \\ W_N \\ \vdots \\ W_N \end{pmatrix} \right) \begin{pmatrix} \xi_N \\ \dot{\xi}_N \\ \vdots \\ \overset{(K)}{\xi}_N \end{pmatrix}$$

$$(3)$$

where the $(K+1)N \times (K+1)N$ matrix Φ contains the basis vectors of the extended subspace, the subvector ξ_N contains the set of Kth degree *Taylor-Fourier coefficients*, and the subvectors $\overset{(k)}{\xi}_N, k = 1, \ldots K$ their progressive derivatives. Note that the extension entails a cyclic prolongation of the signal model, from $C = 1$ to $C = K + 1$ fundamental cycles.

Due to the obliquity introduced by the Taylor terms, the extended bases are no longer orthogonal, and therefore, for $K \geq 1$, a pair of biorthonormal bases is needed for the orthogonal projection [19]: one basis for the anti-transform in (3), and its dual for the transform:

$$\widehat{\xi} = \widetilde{\Phi}^H x \qquad (4)$$

where $\widetilde{\Phi}$ is the dual matrix given by

$$\widetilde{\Phi} = \Phi \left(\Phi^H \Phi \right)^{-1} \qquad (5)$$

such that $\widetilde{\Phi}^H \Phi = I$.

In [20] the matrix Φ_K in (3) was factorized as:

$$\Phi_K = \Upsilon_K \Omega_K$$

$$= \begin{pmatrix} I & T_1 & \cdots & \frac{1}{K!}T_1^K \\ I & T_2 & \cdots & \frac{1}{K!}T_2^K \\ \vdots & \vdots & \ddots & \vdots \\ I & T_C & \cdots & \frac{1}{K!}T_C^K \end{pmatrix} \begin{pmatrix} W_N & 0 & \cdots & 0 \\ 0 & W_N & \cdots & 0 \\ \vdots & \vdots & \ddots & \vdots \\ 0 & 0 & \cdots & W_N \end{pmatrix}$$

$$(6)$$

in which squared submatrices $T_i, i = 1, 2, \ldots, C$ are the descending $N \times N$ diagonal submatrices of diagonal matrix T in (3). Notice that $\frac{1}{k!} T_i^k$ contains the i-th cyclic piece of the k-th Taylor term. In this factorization, the Taylor-Fourier operator Φ_K is clearly separated in two matrices: Ω_K for the Fourier operator, and Υ_K for the Taylor one.

This factorization was proposed in [20] to reduce the calculations of $\widetilde{\Phi}$, since for the factored form we have:

$$\widetilde{\Phi} = \Upsilon \left(\Upsilon^H \Upsilon \right)^{-1} \frac{\Omega}{N} = \widetilde{\Upsilon} \frac{\Omega}{N}. \tag{7}$$

In this paper, the formulation of the DTFT in (7) is proposed as a way to design lowpass filters (maximally flat lowpass differentiators) in $\widetilde{\Upsilon}$. Notice $\widetilde{\Phi}$ preserves the structure of (6), since vectors of $\widetilde{\Upsilon}$ are linear combinations of vectors in Υ. In consequence, vectors in $\widetilde{\Phi}$ are simply harmonic modulations of the vertical subdiagonals of $\widetilde{\Upsilon}$. In other words, this factorization proves that the baseband subset in $\widetilde{\Upsilon}$ are the envelopes of the corresponding subset of vectors at the harmonic frequencies in the DTFT.

This contribution is important for applications where the energy is present in a few number of frequencies. This is the case of power system signals, since in the synchrophasor application, only the filters at the fundamental frequency are needed, since they reject the harmonic frequencies; and in the power oscillation application, only a set of filters is needed per mode. In these applications, the DTFT is implemented with a huge reduction of computational complexity, since it is reduced to a small number of Finite Impulse Response (FIR) filters. If we need to estimate up to the second derivatives, we need 3 FIR filters of $(K + 1)N$ length per observed frequency.

Concerning the noise sensitivity of the DTFT filters, it can be said ([15], [17], [18]) that for signals with signal to noise ratio (SNR) above 60 dB, the parametric normalized mean-squared errors are negligible.

A. Approximation Error

The best approximated signal through the DTFT decomposition is obtained through the orthogonal projection P matrix. We have:

$$\widehat{x} = \Phi \widehat{\xi} = \Phi \widetilde{\Phi}^H x \tag{8}$$

The Pythagorean theorem holds for the approximation error $e = x - \widehat{x}$, with

$$||e||^2 = ||x||^2 - \widehat{\xi}^H \Phi^H \Phi \widehat{\xi} \tag{9}$$

and normalizing with respect to the signal energy,

$$||\epsilon||^2 = 1 - \frac{\widehat{\xi}^H \Phi^H \Phi \widehat{\xi}}{||x||^2}. \tag{10}$$

The former mean squared error considers the error of the projection onto the whole subspace, i.e. the subspace spanned by the whole set of basis vectors in Φ.

It is also possible to measure the approximation error of the projection onto the subspace spanned only by the basis vectors associated with the fundamental frequency, or fundamental subspace. This can be done by taking the submatrix Φ_1 that contain

those vectors, and the subvector with the corresponding ξ_1 estimates. This measure will be referred to as the *Total Phasor Error* (TPE), since it measures the energy of the given signal left by the fundamental resultant in that subspace. This in turn corresponds to the *Total Distortion* (TD) associated with the captured fundamental component. We thus have:

$$||\epsilon_1||^2 = 1 - \frac{\widehat{\xi_1}^H \Phi_1^H \Phi_1 \widehat{\xi_1}}{||x||^2}. \tag{11}$$

For a given signal, the best phasor estimator is thus the one that minimizes the TPE. As can be seen, the TPE definition is the more general of distortions, since it takes into account any kind of spectral energy present in the signal: subharmonic, interharmonic, and any kind of spectral noise. For periodic signals, TPE is reduced to the Total Harmonic Distortion (THD) [21], and for oscillatory fundamental components, as the test signals of the IEEE synchrophasor Standard [3], the TPE is reduced to the Total Vector Error (TVE). One of the strong limitations of the TVE is that its formulation can only be obtained for signals whose dynamic phasor is theoretically known *a priori*. With a broader definition, TPE can be used to compare phasor estimating algorithms, without knowing the underlaying dynamic phasor of the given signal. In addition, TPE has other two advantages: it depends on the whole set of estimated parameters $\widehat{\xi}$, and it can be calculated for intervals of duration lower than the time interval used in the estimation.

B. Impulse and Frequency Responses of DTFT filters

When K increases, DTFT signal models provide a series of successive approximation subspaces V_K, forming a ladder of spaces [22, Ch. 5] with a nested order: $V_0 \subset V_1 \subset V_2 \cdots \subset V_K$, starting with the central subspace V_0 of the DFT, and progressing as $V_K = V_{K-1} \oplus W_{K-1}$, where W_{K-1} is the orthogonal complement of V_{K-1} in V_K. Thus, starting from a coarse approximation, they gradually offer higher resolution approximations. The main difference between the DTFT and wavelet multi-resolution analysis is that O-splines split the spectrum in uniform bands, centered at harmonic frequencies, while wavelets do it in dyadic bands.

As the impulse responses of the DTFT filters at each harmonic frequency are simply modulated version of the lowpass ones, we focus our attention in these filters to understand the evolution of the DTFT operators.

The top plot of Fig. 1 shows the impulse responses of the lowpass filters for different Taylor degrees $K = 0, 1, \ldots, 11$. They were calculated with $N = 20$ samples per fundamental cycle. It can be shown from (7) that they form a new family of splines of $C = K + 1$ cycles. The first two correspond to the zeroth and first B-splines [23, Ch.10], but then they differ for $K \geq 2$, since they converge to the *Cardinal Sine*, as can be corroborated in the plot by the curve of $K = 11$. They start with the rectangular window, corresponding to the traditional one-cycle Fourier filter, then the two-cycle triangular window, as the P class filter example in the IEEE standard [3, C.5.1], then their shapes evolve up to the *sinc* function, as $K \to \infty$. In fact, the 5th one of 6 cycles, is very similar to the M class filter example in the IEEE standard [3, C.6].
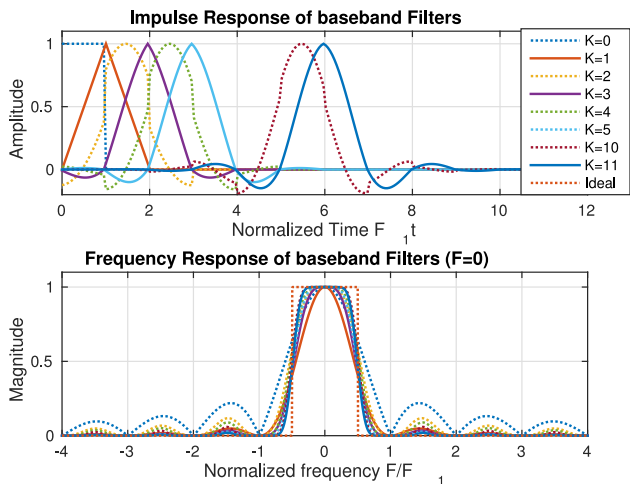
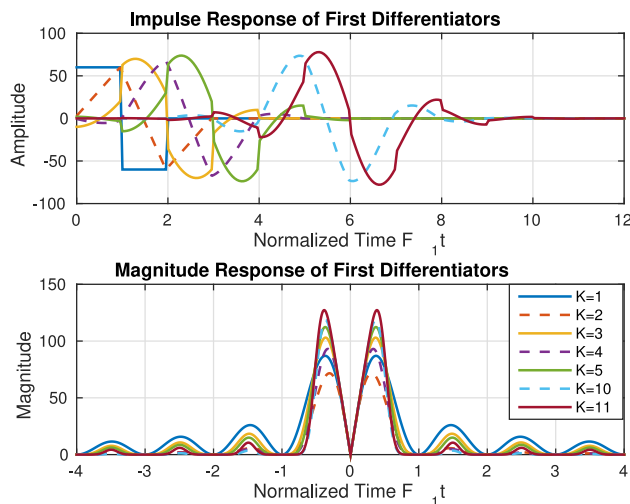Fig 1. Impulse and Frequency responses of the lowpass filters, $K = 0, 1, \ldots, 5$, and 11.

Fig 2. Impulse and magnitude responses of the first lowpass differentiators, $K = 0, 1, \ldots, 5$, and 11.

Fig 3. Impulse and magnitude responses of the second lowpass differentiators, $K = 0, 1, \ldots, 5$, and 11.
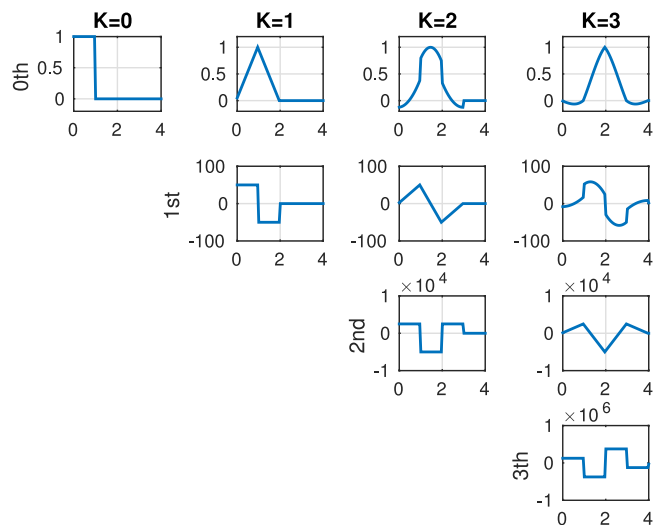
Fig 4. Impulse responses (O-splines) of the lowpass DTFT differentiators, for $K = 0, 1, 2, 3$.

The advantage of the DTFT filters is that they come together with the baseband differentiators, which are also splines. Because of their cyclic nature, these new family of splines will be referred to as O-splines. The bottom plot of Fig. 1 illustrates the spectra of the O-splines. As we can see, the sequence starts with the *Cardinal Sine* function of the rectangular window, followed by its squared function, corresponding to the triangular window. After that, they start having flatter passbands, and zero flatter stopbands. This feature is very important to reject harmonic interferences. As the Taylor degree K increases, the frequency responses of the O-splines tend to an ideal baseband filter. Notice that these DTFT filters provide a new sequence of approximation to the ideal filter, similar to those of the Butterworth or Raised Cosine ones. But DTFT filters include their own differentiators too, as seen in the following subsection.

C. Passband Differentiators

The top curve of Fig. 2 shows the impulse responses of the first lowpass differentiators. Note that they are discontinuous
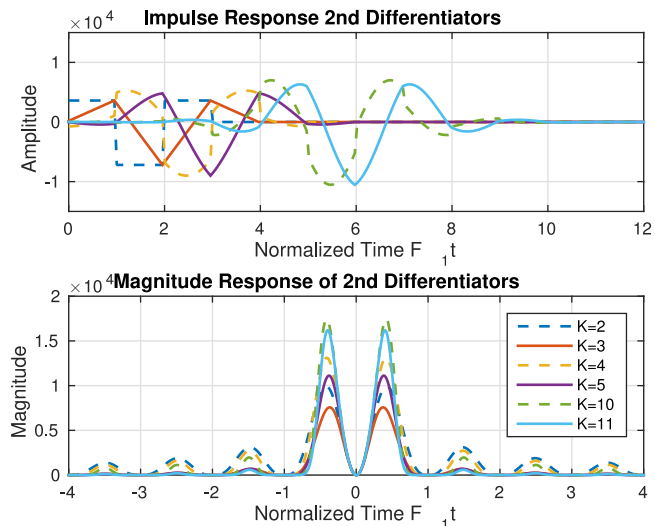
splines, which are obtained from the first derivative of the former ones. Their frequency response are plotted at the bottom. Note that if $H_k^{(0)}(f)$ is the frequency response of the k-th lowpass filter, then the frequency response of the corresponding first differentiator is $H_k^{(1)}(f) = (j2\pi f)^1 H_k^{(0)}(f)$, and then their frequency responses have a linear gain in their passband. Finally, note that the even filters have higher sidelobes than those of the odd-ones.

Similarly, the impulse responses of the second differentiators are shown in the top curve of Fig. 3. Again, they are discontinuous splines, which are the derivative of the precedent ones. Their frequency responses are plotted on the bottom plot. These have a parabolic gain at the passband since $H_k^{(2)}(f) = (j2\pi f)^2 H_k^{(0)}(f)$.

Finally, the plots in the columns of Fig. 4 illustrate the impulse responses of consecutive DTFT differentiators, from $K = 0$ to $K = 3$. As can be seen, higher degrees require wider observation
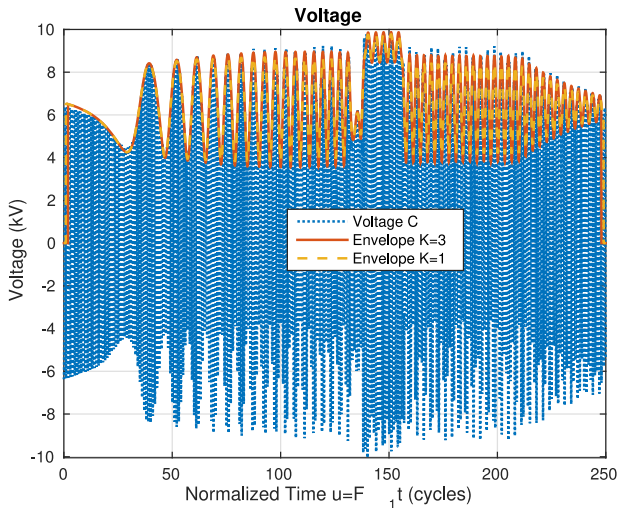
Fig 5. Voltage C during a power swing (dotted line), and amplitude envelopes point wise estimated with a DTFT with $K = 3$ (continuous line), and $K = 1$ (dashed line).
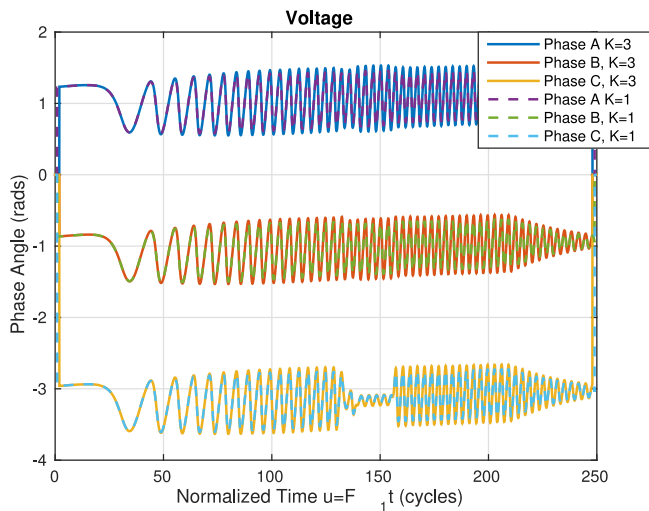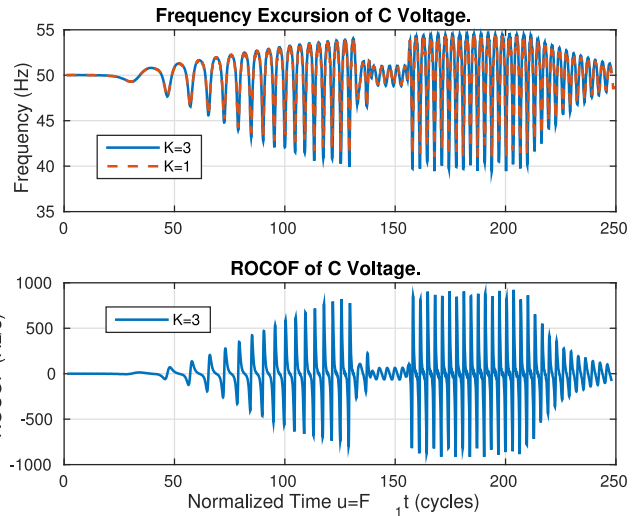

Fig 7. At the top plot, frequency of C voltage during the swing, continuous line ($K = 3$), and dashed line ($K = 1$). At the bottom, ROCOF estimated with $K = 3$.
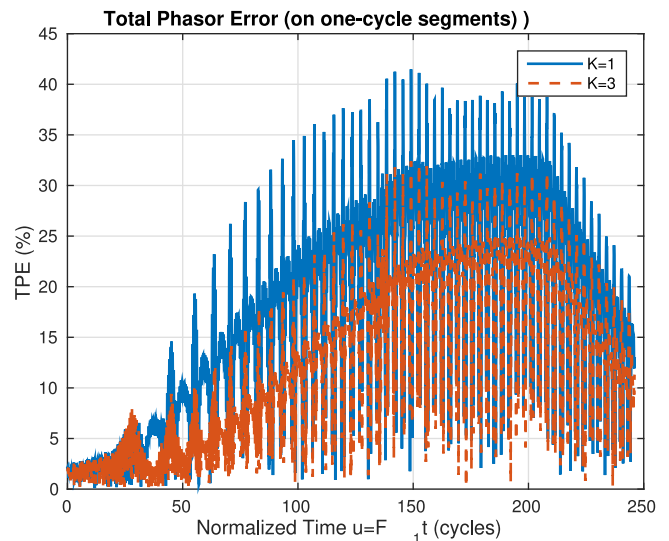

Fig 6. Phase angle of A, B, and C voltages, during the power oscillation in Fig. 5, with $K = 3$ (continuous line), and $K = 1$ (dashed line).

Fig 8. TPE calculated over one-cycle intervals, with $K = 1$ and $K = 3$.

windows, since they deliver more details of the dynamic events, and improve parametric accuracy. In the following section, we compare the synchrophasors and estimated parameters with the set of differentiators obtained from the first and third degree Taylor polynomials.

III. SYNCHROPHASOR ESTIMATION

Estimation of dynamic phasors in power systems is an interesting application of the DTFT. With the DTFT is possible to estimate not only the excursions of amplitude and phase of voltages and currents during a power system oscillation, but also their frequency fluctuations, and their rate of change (ROCOF). In this section we will illustrate the estimates of three-phase voltages of an interesting real oscillation case from a real 50 Hz power system, whose signals were recorded at 20 samples per fundamental period (1 kHz).

Fig. 5 shows the Voltage C signal during a fast power swing (dotted line), together with the estimated envelopes, obtained

with $K = 1$ and $K = 3$, respectively. The estimates are calculated by sliding the observation window point by point, producing *pointwise* estimates. On the other hand, Fig. 6 shows the phase estimates of the three voltages. As can be seen, the oscillation case corresponds to a very fast swing.

The derivative of the phase angle provides the frequency fluctuation during the oscillation. The plot at the top of Fig. 7 shows the frequency estimates of the C voltage signal. The crossings at the line $f = 50$ Hz mark the maxima and minima points of the phase plot in Fig. 6. It is apparent that the DTFT analysis can track very fast and large frequency excursions (larger than the bounds of the Standard). On the other hand, the bottom plot in Fig. 7 illustrates the ROCOF of the event in Hz/s. Again, its zero crossings mark the maxima and minima of the frequency fluctuation in the top plot.

Finally, Fig. 8 shows the TPE defined in (11), calculated over intervals of one-cycle, between the given signal and the estimated bandpass signal, synthesized with the instanta-
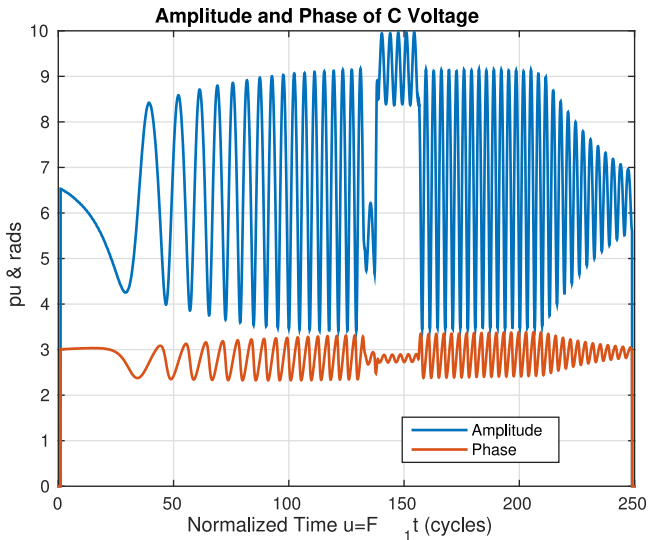
Fig 9. C-Voltage amplitude and phase estimates with compressed 3rd O-splines of 2-cycles.

Fig 10. TPE in C-Voltage with compressed 3rd O-splines of 2-cycles.

neous pointwise estimates. As expected, the errors with $K = 1$ are higher than those with $K = 3$, however both approximations are poor. Apparently, an anomalous signal was found for the DTFT. Notice that the peak errors in Fig. 8 are due to the frequency slumps in Fig. 7, and that better approximations are found below the tops of its concave fluctuations. In addition, the frequency parabolic shapes are becoming narrower as time goes on, from 10 to 3 fundamental cycles. Since the used O-spline is 4 periods long, the smooth assumptions are only met when the parabolic fluctuations are wider than 4 cycles. This explains the increasing error in Fig. 8 until the larger ones, obtained after the 150th cycle.

Fortunately, DTFT provides a wide range of solutions. The former inconvenient is solved by downsampling the 3rd O-splines by a factor of 2, and rescaling them to achieve unit gain in the lowpass filter. In this way, the O-splines are now much narrower (2-cycles long). Fig. 9 shows amplitude and phase estimates from the C-Voltage with these time-compressed O-splines. This change reduces the TPE as shown in Fig. 10. Notice that the strong parabolic frequency fluctuations are still apparently manifested in this plot.

IV. POWER SYSTEM OSCILLATION MODES IN SMART GRIDS

In this section the 3rd DTFT is used to identify the electromechanical modes [15] of the power oscillation of the precedent swing. As the frequencies of the modes must be known *a priori*, this application is still for *post mortem* analysis. This application shows that DTFT is able to detect frequency modulated modes.

The instantaneous power oscillation appears at the top plot of Fig. 11, and its normalized spectrum is illustrated at the middle. It contains a mode at $f_0 = 0$, and another one at $f_1 = 15.7$ Hz. The oscillation also has three small modes at higher frequencies. One at $f_2 = 100.48$ Hz, other at $f_3 = 113.04$ Hz, and the last one at $f_4 = 128.74$ Hz. As can be seen, the frequencies of these modes are not integer multiples of the first one (at 15.7 Hz).
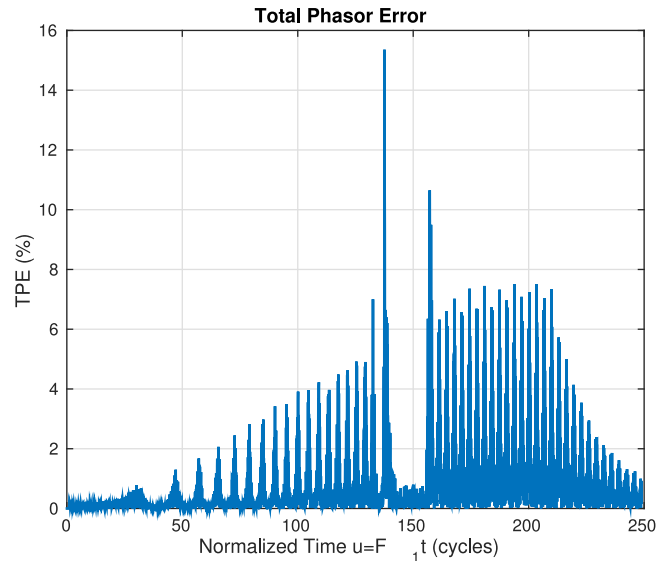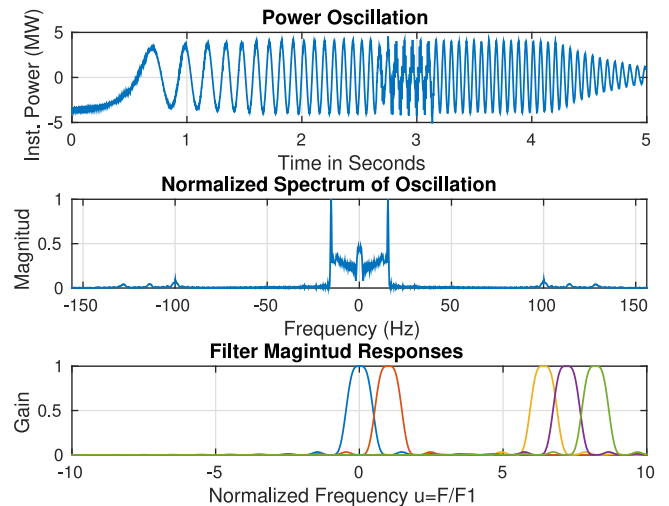

Fig 11. Instantaneous Power Oscillation (top), its normalized spectrum (middle), and the magnitude response of the DTFT filters (bottom).

The plot at the bottom illustrates the magnitude response of the DTFT filters used in the analysis. They were designed as follows: One fundamental cycle of the power oscillation (64 ms) contains 64 samples. Then the DTFT must include 32 harmonics. The time observation window of the filters is therefore of 256 ms. The three passband filters at high frequencies are tuned at the central frequency of the corresponding mode.

Fig. 12 shows the estimated modes, and at the bottom the reconstructed power oscillation with the original one. The sequence of each mode m is calculated from its instantaneous Taylor-Fourier coefficient $\xi_m(n)$ simply as $s_m(n) = 2|\xi_m(n)|\cos(\angle\xi_m(n))$, since the contribution of the derivatives greater than zero $\xi_m^{(k>0)}(n)$ at the center of the interval is zero. As can be seen, the zeroth mode lasts about the first 2 seconds, and the first mode during the last 4 seconds, whereas the rest of the modes live only during half a second after the middle of the time interval. These plots show how the DTFT is capa-
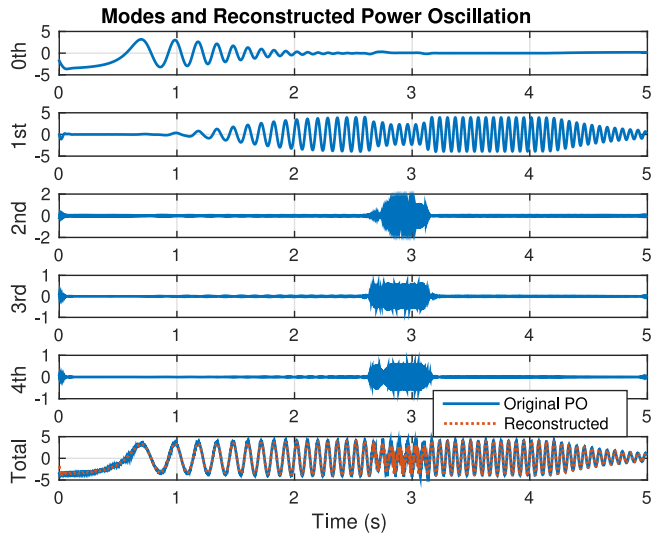
Fig 12. The modes, and the reconstructed power oscillation at the bottom plot, compared with the original oscillation.
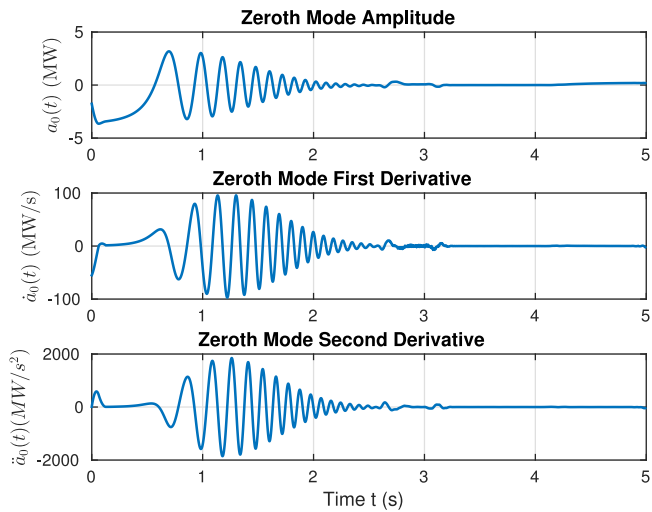

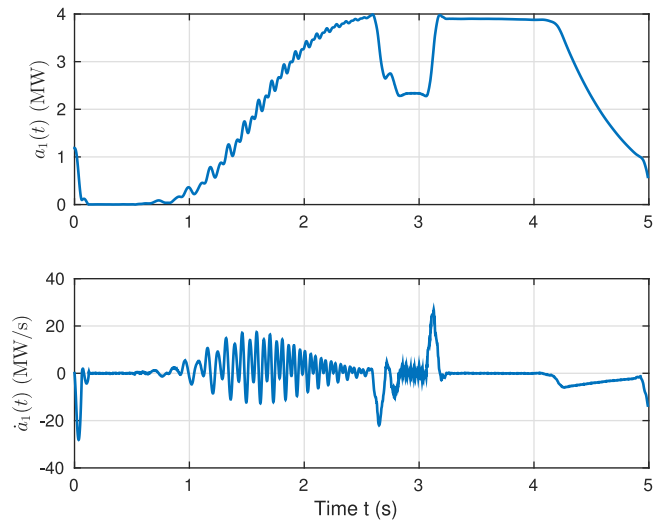Fig 13. Zeroth mode amplitude, and its first two derivatives.

Fig 14. Amplitude envelope of the first mode in MW (top plot), and its first derivative in MW/s.
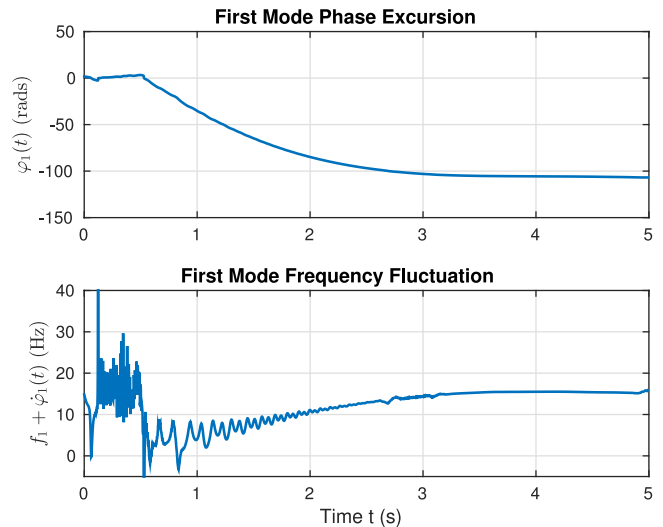
Fig 15. Phase (top plot) and frequency (bottom plot) of the first mode.

ble of separating time-frequency events. It divides the whole event in three successive disjoint intervals: the one before the fault, the short time interval of the fault, at the middle of the plot, and the last one after the fault. At the bottom plot, it is apparent that the reconstructed power oscillation fits (dotted line) well the given power oscillation. The energy of the approximation error is 5% of the energy of the power oscillation signal. There is a small error due to the fact that the first two modes are not perfectly separated, i.e. they share energy under the transition bands of the corresponding filters (see Fig. 11).

Traditional decomposition mode techniques usually consider the zeroth component as a constant to be removed by subtracting its mean from the whole oscillation before the analysis. This consideration is a heritage of the Fourier way of thinking. The DTFT mode decomposition clearly shows that, in general, the zeroth mode fluctuates, and must be considered as an oscillatory mode *per se*, since it contains important dynamic information, as it will be seen in what follows.

The zeroth mode amplitude and its first derivatives are shown in plots of Fig. 13. Notice that zero-crossings of first derivative correspond to the *maxima* and *minima* values of the amplitude oscillation. The same is valid for the second derivative. The DTFT derivatives are very accurate.

Moreover, Fig. 14 shows, in its top plot, the amplitude envelope of the first mode in MW, and at the bottom its first derivative, in MW/s. There is an apparent infiltration from the zeroth mode, which is amplified by the first differentiator. When this mode disappears (post fault interval), the amplitude envelope and its derivative become smooth. Notice that two peaks delimit the duration of the fault.

On the other hand, the top plot of Fig. 15 shows the phase, and its derivative at the bottom. Again, the zero mode infiltration is apparent in the bottom plot. However, it is also evident that the first mode is frequency modulated, since its frequency starts at zero Hz, and gradually increases with fluctuations up to
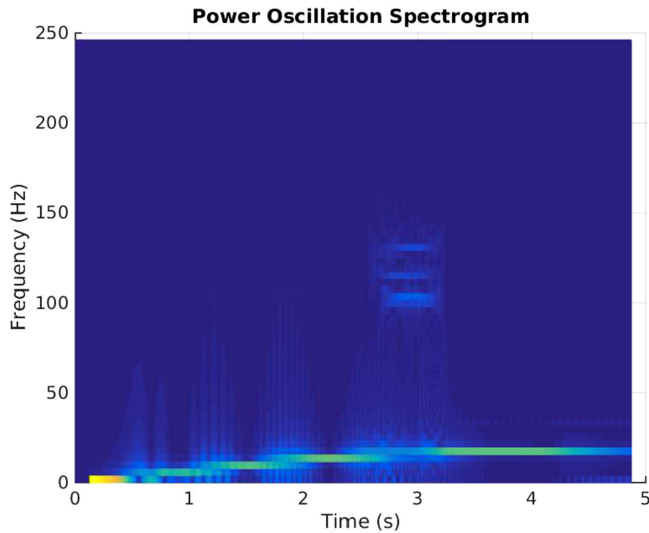
Fig 16.   Power oscillation spectrogram.

15.6 Hz at $t = 3$ s, and maintained until the end of the record. The frequency elevation is also shown with less resolution in the spectrogram of the power oscillation illustrated in Fig. 16, calculated with a sequence of Fast Fourier Transforms (FFTs) using a rectangular window of 256 samples. The frequency variation is also apparent in the power oscillation itself, in Fig. 11, in which the peak to peak time intervals are diminishing. Thus DTFT discovers a dynamic frequency not perceived by the traditional mode decomposition methods, which assume constant frequency modes.

The same estimates can also be obtained for the three modes in the fault. But the analyzed modes are enough to show that DTFT provides time-frequency separation, and can deal with frequency modulated modes. In [15] the performance of the 3rd DTFT analysis was compared with that of Prony [10], Eigensystem Realization Algorithm [24], and Matrix Pencil [25] methods. From the inter-area modes analyzed in [15] (at 0.133, 0.399, 0.532, 0.665, and 0.798 Hz), it was concluded that DTFT can be applied to low-frequency oscillations. Nevertheless, note that the analysis of lower frequency modes require longer windows; for example, a mode at 0.1Hz needs a time window of 40 s.

V. Discussion

With respect to the synchrophasor application, the O-splines provide a series of elegant solutions for P and M class applications. The results show that DTFT estimates provide richer dynamic information than the specified by the IEEE Synchrophasor Standard. In addition, TPE assesses the quality of the estimated parameters. Concerning the problem of detection of oscillation modes, the DTFT provides time-frequency separation of frequency modulated modes. Finally, the elegant mathematical theory behind DTFT offers a unifying solution for two important problems in wide-area power systems measurements, traditionally considered as completely independent problems. However, DTFT assumes that the spectral energy of the signal is concentrated about certain frequencies, and that

in the time window the complex envelope is smooth as to be differentiable (Taylor assumptions). Thus, DTFT is unable to extract a quick transient with a broad spectrum, since it would split it in several components.

VI. Conclusion

O-splines allow to tune DTFT filters only at a certain number of required frequencies, reducing the computational complexity of the whole DTFT. Taylor-Fourier coefficients are very useful for multi-resolution analysis of oscillating signals with frequency fluctuations. Our signal case illustrates that there are real power signals with much more complex fluctuations than those of the bench signals of the IEEE Synchrophasor standard. Concerning the oscillation mode separation problem, DTFT is able to separate, and locate in time, frequency modulated modes, including the oscillatory zeroth mode.

A unifying theory solves two important power system problems, and opens the way to more complete and accurate interpretations of the events (new knowledge). The next stage is to use O-splines with frequency adaptation, and real time solutions for the separation of power oscillation modes.

References

[1] J. G. Proakis and D. K. Manolakis, *Digital Signal Processing*, 4th ed. Upper Saddle River, NJ, USA: Pearson, 2006.

[2] M. A. Platas-Garza and J. A. De la O Serna, "Dynamic harmonic analysis through Taylor–Fourier transform," *IEEE Trans. Instrum. Meas.*, vol. 60, no. 3, pp. 804–813, Mar. 2011, doi: 10.1109/TIM.2010.2064690.

[3] *IEEE Standard for Synchrophasor Measurements for Power Systems* IEEE Std C37.118.1, 2011.

[4] A. G. Phadke and B. Kasztenny, "Synchronized phasor and frequency measurement under transient conditions," *IEEE Trans. Power Del.*, vol. 24, no. 1, pp. 89–95, Jan. 2009.

[5] R. Ghiga, K. Martin, Q. Wu, and A. Nielsen, "Phasor measurement unit test under interference conditions," *IEEE Trans. Power Del.*, vol. 33, no. 2, pp. 630–639, Apr. 2018, doi:10.1109/TPWRD.2017.2691356.

[6] D. Macii, D. Petri, and A. Zorat, "Accuracy analysis and enhancement of DFT-based synchrophasor estimators in off-nominal conditions," *IEEE Trans. Instrum. Meas.*, vol. 61, no. 10, pp. 2653–2664, Oct. 2012.

[7] M. Karimi-Ghartemani, B. T. Ooi, and A. Bakhshai, "Application of enhanced phase-locked loop system to the computation of synchrophasors," *IEEE Trans. Power Del.*, vol. 26, no. 1, pp. 22–32, Jan. 2011.

[8] I. Kamwa, A. K. Pradhan, and G. Joos, "Adaptive phasor and frequency-tracking schemes for wide-area protection and control," *IEEE Trans. Power Del.*, vol. 26, no. 2, pp. 744–753, Apr. 2011.

[9] J. S. Gasca and D. Trudnowski, "Identification of electromechanical modes in power systems," IEEE Power and Energy Society, Task Force on Identificatioin of electromechanical modes, Tech. Rep. PES-TR15, Jun. 2012, [Online]. Available: http://resourcecenter.ieee-pes.org/pes/product/technical-publications/PESTR15

[10] J. F. Hauer, C. J. Demeure, and L. L. Scharf, "Initial results in Prony analysis of power system response signals," *IEEE Trans. Power Syst.*, vol. 5, no. 1, pp. 80–89, Feb. 1990.

[11] J. Rommes, N. Martins, and F. Freitas, "Computing rightmost eigenvalues for small-signal stability assessment of large scale power systems," in *Proc. IEEE Power Energy General Meeting*, Jul. 2010, pp. 1–1.

[12] J. W. Pierre, D. J. Trudnowski, and M. K. Donnelly, "Initial results in electromechanical mode identification from ambient data," *IEEE Trans. Power Syst.*, vol. 12, no. 3, pp. 1245–1251, Aug. 1997.

[13] A. R. Messina and V. Vittal, "Nonlinear, non-stationary analysis of inter-area oscillations via Hilbert spectral analysis," *IEEE Trans. Power Syst.*, vol. 21, no. 3, pp. 1234–1241, Aug. 2006.

[14] A. Q. Zhang, L. L. Zhang, M. S. Li, and Q. H. Wu, "Identification of dominant low frequency oscillation modes based on blind source separation," *IEEE Trans. Power Syst.*, vol. 32, no. 6, pp. 4774–4782, Nov. 2017.

[15] J. A. De la O Serna, J. M. Ramirez, A. Zamora Mendez, and M. R. A. Paternina, "Identification of electromechanical modes based on the digital Taylor–Fourier Transform," *IEEE Trans. Power Syst.*, vol. 31, no. 1, pp. 206–215, Jan. 2016, doi: 10.1109/TPWRS.2015.2403290.

[16] J. A. De la O Serna, "Synchrophasor measurement with polynomial phase-locked-loop Taylor–Fourier filters," *IEEE Trans. Instrum. Meas.*, vol. 64, no. 2, pp. 328–337, Feb. 2015, doi: 10.1109/TIM.2014.2344333.

[17] J. A. De la O Serna, "Dynamic phasor estimates for power system oscillations," *IEEE Trans. Instrum. Meas.*, vol. 56, no. 5, pp. 1648–1657, Oct. 2007, doi: 10.1109/TIM.2007.904546.

[18] M. A. Platas-Garza and J. A. De la O Serna, "Dynamic phasor and frequency estimates through maximally flat differentiators," *IEEE Trans. Instrum. Meas.*, vol. 59, no. 7, pp. 1803–1811, Jul. 2010, doi: 10.1109/TIM.2009.2030921.

[19] M. Vetterli, K. Kovacevic, and V. K. Goyal, *Foundations of Signal Processing*, 3rd ed. Cambridge, U.K.: Cambridge Univ. Press, 2014. [Online]. Available: http://www.fourierandwavelets.org/

[20] J. A. De la O Serna, "Taylor–Fourier analysis of blood pressure oscillometric waveforms," *IEEE Trans. Instrum. Meas.*, vol. 62, no. 9, pp. 2511–2518, Sep. 2013, doi: 10.1109/TIM.2013.2258245.

[21] D. Shmilovitz, "On the definition of total harmonic distortion and its effect on measurement interpretation," *IEEE Trans. Power Del.*, vol. 20, no. 1, pp. 526–528, Jan. 2005.

[22] I. Daubechies, *Ten Lectures on Wavelets*. Philadelphia, PA, USA: SIAM, 1992, doi: 10.1137/1.9781611970104.

[23] O. Christensen, *Functions, Spaces, and Expansions*. Berlin Germany: Springer, 2010.

[24] J. N. Juang and R. S. Pappa, "An eigensystem realization algorithm for modal parameter identification and model reduction," *J. Guid., Control, Dyn.*, vol. 8, no. 5, pp. 620–627, 1985, doi: 10.2514/3.20031.

[25] Y. Hua and T. K. Sarkar, "Matrix pencil method for estimating parameters of exponentially damped/undamped sinusoids in noise," *IEEE Trans. Acoust., Speech, Signal Process.*, vol. 38, no. 5, pp. 814–824, May 1990.

José Antonio de la O Serna (SM'03) received the Ph.D. degree from Telecom ParisTech, Paris, France, in 1982. In 1987, he joined the Ph.D. program in electrical engineering with the Autonomous University of Nuevo Leon (UANL), Monterrey, Mexico, where he is currently a Research Professor. From 1982 to 1986, he was also a Professor with Monterrey Institute of Technology. From 1988 to 1993, he was with the Electrical Department, Polytechnic School in Yaounde, Cameroon. He is the Member of the Mexican Research System.